Research paper

An analytical method for calculating the natural frequencies of spatial compliant mechanisms

Vivien Platl [*], Lena Zentner

Compliant Systems Group, Department of Mechanical Engineering, Technical University Ilmenau, P.O. Box 100565, 98693, Ilmenau, Germany

ARTICLE INFO

ABSTRACT

Compliant mechanisms are becoming increasingly important in both research and industry. The design and the static analysis of such mechanisms has made much progress in recent years, yet comparatively little research has been done on their dynamic behaviour. The aim of this paper is to advance the dynamic analysis of spatial compliant mechanisms by pursuing the calculation of their natural frequencies. So far, their determination is only possible with time-consuming 3D-FEM simulations or via pseudo-rigid-body models and Lagrangian equations. An analytical method is developed to simplify and accelerate the calculation of the natural frequencies of compliant mechanisms. The method is integrated into an algorithm on which a graphical user interface is developed to allow the design and calculation of the system in the most time efficient and intuitive way. The results are verified by 3D-FEM simulations and validated through an experiment. The evaluation shows good agreement with the reference models. The results of this paper allow a reliable and efficient calculation of natural frequencies and serve to facilitate further work regarding the dynamic analysis of compliant mechanisms.

1. Introduction

Due to the advantages of zero backlash, maintenance and friction of compliant mechanisms, they are increasingly replacing conventional rigid-body mechanisms, especially in precision engineering and precision mechanics, but also in classical mechanical engineering [1]. While much progress has been made in recent years in the static analysis, synthesis [2] and design [3] of such systems, little research has been done on their dynamic behaviour.

Especially for systems subjected to high dynamic processes, such analysis is indispensable. This includes, for example, the investigation of compliant mechanisms with respect to their natural frequencies. Most systems have an operating frequency and assessing that the compliant mechanisms natural frequencies are not within its range ensures a faultless operation. Integrating a mechanism whose natural frequency is close to the operating frequency of the whole system can lead to resonance and eventually to its failure and destruction. Therefore, gaining knowledge of the natural frequencies already in the design process and before the actual manufacturing and assembly process helps to save lots of money and time. It further allows to draw conclusions about their suitability and integrability for/in corresponding system(s).

So far, finite element models and simulations [4–9] and pseudo-rigid-body models (PRBM) [10–15], possibly combined with the Lagrange equation, are the most common methods to investigate the dynamic behaviour of compliant mechanisms. An overview is given in Table 1. Depending on various boundary conditions, such as the discretisation, the degrees of freedom of the elements used and the overall model, the calculation can thus be fast or time and computationally intensive. Especially the creation of complex mechanisms and whole series of experiments take a lot of time.

---

* Corresponding author.
E-mail addresses: vivien.platl@tu-ilmenau.de (V. Platl), lena.zentner@tu-ilmenau.de (L. Zentner).

Table 1

Overview of analytical models for the dynamic analysis of compliant mechanisms — PRBM: pseudo rigid body model, FEM: finite elements method, TMM: transfer matrix method, LG: Lagrange equations, BT: beam theory, FH: flexure hinge, CM: compliant mechanism, S: serial, B: branched, EF: eigenfrequency, dev.: deviation of the first natural frequency to comparative value, the * indicates, that the tool is no stand-alone program and that a MATLAB licence is required.

Ref.	Model					Tool	Object	Mech.		Input		Output		Dev.
	PRBM	FEM	TMM	LG	BT			2D	3D	Free	Other	EF	Other	[%]
[4]		x				x*	CM	S/B	S/B	x	x	x	x	–
[5]		x		x			CM/FH	S/B		x	x	x	x	6.2
[6]		x					CM/FH		S	x		x		9.7
[7]		x		x			CM	B			x	x	x	–
[8]		x					CM	S		x		x	x	1.1
[9]		x					CM	B			x	x	x	6
[10]	x			x			CM	S		x		x	x	2.8
[11]	x			x			CM	S		x		x		8
[12]	x			x			CM	S/B		x		x		2.2
[13]	x			x			CM/FH	S		x		x		12
[14]	x					x*	CM	S		x		x		0.2
[15]	x			x			CM	S		x		x		5.5
[16]	x			x			CM			x		x		2.1
[17]			x				CM/FH	S/B		x	x	x	x	5
[18]			x				CM/FH	S/B			x	x	x	6
[19]					x		CM/FH	S		x		x		8.7
CaTEf				x	x		**CM/FH**	**S**	**S**	**x**		**x**		**<5**

The subject of this work is the development of a time-effective and widely applicable analytical model and its integration into a freely accessible calculation tool. It helps to save time and resources in the development and fabrication of technical products. This can enable considerable cost and time saving, because no FEM simulations and/or experiments are needed. It helps to detect possible issues due to resonance and undesired vibrations in advance.

Different approaches and methods can be found, which study specific or a whole class of compliant mechanisms in terms of their dynamics. A thorough survey regarding the kinetostatic and dynamic modelling of flexure-based compliant mechanisms is presented in [20].

The first paper on determining the first natural frequency of a compliant mechanism using the PRBM was published in 1999 in [11]. Their analysis is limited to the first natural frequency of the mechanisms and deviations of up to 9% are found through experiments. In [12], also using a PRBM, the dynamic behaviour of a parallel crank and beam is studied. The deviations of the natural frequencies, compared to results calculated using the finite element method (FEM), are around 2%. Another approach of the analysis of the free oscillations of plane compliant mechanisms is proposed in [13]. The mechanisms there have serially installed solid-state joints. The method is based on a PRBM and the joints have three degrees of freedom. Using a modified PRBM, a compliant parallel guide and a compliant bistable mechanism are investigated in [10]. The PRBM for static and kinetic conditions is adapted to make it more suitable for studying the dynamic behaviour of the mechanisms.

A dynamic pseudo rigid body model (PRBDM), which allows the dynamic analysis of compliant unilaterally restrained beams, was developed in [14]. Their method fits the dynamic response of the PRBDM to the expected response of the yielding system. The natural frequencies for the study are determined via the eigenvalue analysis of the COMSOL program. The eigenvalues of the PRBDM equations are adjusted using an optimisation scheme to find the system parameters that minimise the difference in the eigenvalues of the two systems.

The model in [15] is also based on the dynamic pseudo rigid body model (PRBDM). Unlike in [14] however, the approaches are not fitted to an expected result in order to arrive at the most accurate solution possible, but are obtained using Lagrange's equations. A system with more degrees of freedom (2R-nR PRBDM) is found to be superior to the system with one degree of freedom. The two-degree-of-freedom model also has the advantages of simplification of the dynamic equations and numerical solutions over the systems with more degrees of freedom. In [16] a dynamic analysis of a hybrid compliant mechanism for hand tremor suppression is carried out. The analytical model is based on Lagrange's equations. For the first natural frequency, deviations of less than 2% are obtained — the calculated results for higher natural frequencies, however, deviate very strongly from the comparative model.

A finite element formulation for multi-degree of freedom mechanisms is presented in [4]. It enables the calculation of static deflection, stress, natural frequencies and critical buckling load of three dimensional structures consisting of beam-like parts. It further serves as the theoretical background to a toolbox called SPACAR. Although it is not explicitly designed for the calculation of compliant systems, it is used in current research projects regarding this topic. The toolbox has no graphical user interface and runs entirely in MATLAB as a script with the input being done via MATLAB commands.

A semi-analytical modelling method for the static and dynamic analysis of complex compliant mechanisms is presented in [5]. It is a finite element model based on Lagrange's equations and includes the calculation of compliant segments, which are both concentrated and distributed and in the form of flexure hinges or segments. To verify the method, the same parallel crank mechanism as from [6] is calculated and the results are considered in comparison with the FE model. The deviations obtained are less than 8%. The approach used in [6] to model semicircular flexure hinges is a spatial force-based finite element method for non-prismatic beam elements.

In [7] an FEM based approach to set up the dynamic differential equations to describe compliant mechanisms is presented. The approach allows the calculation of natural frequencies and a sensitivity analysis. The latter is an effective way to predict the influence of different physical parameters on the performance of the compliant mechanism. The approach from [8] is based on the same modelling as [6]. The authors use this force-based finite element method to calculate a mechanism in the form of a parallel crank and achieve deviations of less than 3% to FEM for the first three natural frequencies.

In [9], an FEM-based model, the significant region model (SRM), is chosen to create small but highly accurate models for flexure hinges and compliant mechanisms. Deviations from the finite element reference model of less than 6% were thus found.

In [17], a dynamic model is proposed that describes the vibration characteristics of planar compliant mechanisms using a transfer matrix method (TTM). The authors distinguish between serial compliant mechanisms, successive chains with compliant and rigid segments, and parallel compliant mechanisms. These have n different sub-chains and rigid bodies. The presented method thus also allows the calculation of double-parallel mechanisms. The deviations of the results from the FE models are a maximum of 5%.

For planar and serial parallel compliant mechanisms, a transfer matrix method combined with d'Alembert's principle is presented in [18]. The dynamic stiffness model for mechanisms with two inputs and one output is derived. For the calculations of the first two natural frequencies, results with deviations from the corresponding FE model of less than 6% are obtained.

Also in [19] a TMM to calculate the natural frequencies in two-dimensional space for serial planar mechanisms is presented. The approach is based on the 2nd Newton's axiom. In [21] the free vibrations of structures with rigid bodies and compliant beam segments is investigated using a transfer matrix method. Although the structures are not referenced as compliant mechanisms, the approach is applicable. The method presented in [19] has already been investigated and refurbished at the Ilmenau University of Technology. It serves as the basis for the analytical model created in this work.

After extensive research, as can be seen in Table 1, the author is not aware of any other stand-alone calculation tools for the analysis of the dynamic behaviour of compliant mechanisms. Both [4,14] propose a MATLAB based code for the analysis of compliant mechanisms. The code by [14] is a reduced-order PRBD model for calculating the natural frequencies of planar compliant cantilever beams with the main objective of reducing computational expense. The finite element method based MATLAB-package SPACAR by [4], can be used for calculating the static deflection, stress, natural frequency and critical buckling load of spatial structures consisting of beam-like parts. It has no graphical-user interface but enables the visual representation of the input done via MATLAB-commands. But neither of these two are stand-alone tools, nor can they be used without a MATLAB licence and are therefore not available to everyone. Furthermore, the inclusion of flexure hinges and branching is not provided for.

The proposed method of analysis of this work, based on the EULER–BERNOULLI-Beam theory, and its inherent possibility to study spatial mechanisms as well as mechanisms with flexure hinges have been very rarely explored so far, as can be seen in Table 1. The resulting tool is novel and hitherto singular. Due to its intuitive graphical user interface, it can be used by almost everyone and no prior knowledge of MATLAB is necessary. This all, together with the very good results obtained with this method, makes the method and tool valuable and unique. It allows the reliable and efficient calculation of natural frequencies and serves to facilitate further work regarding the dynamic analysis of compliant mechanisms.

In this work a new analytical method is presented for the calculation of the natural frequencies of planar and spatial compliant mechanisms (Section 2). It is based on the EULER–BERNOULLI-Beam theory and the transfer matrix method. The method is then implemented into a stand-alone graphical user interface (GUI) as an algorithm (Section 3). Several examples mechanisms with circular and rectangular cross sections, flexure hinges, a varying number of segments and their overall appearance are analysed. For verification (Section 4), the obtained results are compared to the results from literature and other results with FEM simulations and are validated through an experiment. The method and the obtained results are discussed and Section 5 concludes the work.

2. Analytical approach

In the following section the developed analytical approach for the calculation of the natural frequencies of compliant mechanisms is presented. It is based on the EULER–BERNOULLI-Beam theory. This method is later on implemented into a GUI which allows for quick calculation of the natural modes of compliant mechanism without costly FEM simulations and/or experiments.

The natural frequencies of an EULER–BERNOULLI-Beam are calculated by finding the non-trivial solutions of the coefficient matrix of the vibration equations of said beam. In order to solve these equations boundary conditions are needed. If a whole mechanism is considered, instead of just one beam, additional boundary conditions at the connecting point of two consecutive segments are needed — these are called transition conditions. The presented analytical method presents a way of combining the vibration equations of each individual segment of the regarded mechanism. The equations can each be written in coefficient matrix notation and are combined by a matrix multiplication, see Eqs. (9) and (11). The needed boundary conditions are presented in Table 2, and the transition conditions in Eqs. (6)–(7).

2.1. Differential equations of motion

A slender beam segment with the length dx, as shown in Fig. 1 is considered. It has the following properties: density - ρ, cross-sectional area A, elastic modulus E and shear modulus G.
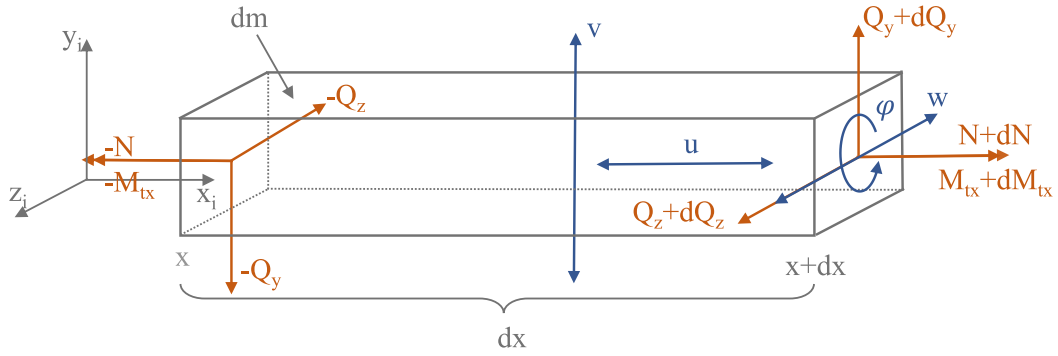
Fig. 1. Beam segment dx for free vibration calculation.

The differential equations for the free transverse and axial vibrations of an elastic Euler–Bernoulli beam, see [22] for reference, with $i = 1, \ldots, n$ are as follows:

$$
\begin{aligned}
a_{wi} \frac{\partial^2 w_i(x,t)}{\partial t^2} + \frac{\partial^4 w_i(x,t)}{\partial x^4} = 0 \qquad & a_{wi} = \frac{\rho A_i}{E I_{yi}} && \text{(transversal in z)} \\
a_{vi} \frac{\partial^2 v_i(x,t)}{\partial t^2} + \frac{\partial^4 v_i(x,t)}{\partial x^4} = 0 \qquad & a_{vi} = \frac{\rho A_i}{E I_{zi}} && \text{(transversal in y)} \\
a_{ui} \frac{\partial^2 u_i(x,t)}{\partial t^2} - \frac{\partial^2 u_i(x,t)}{\partial x^2} = 0 \qquad & a_{ui} = \frac{\rho}{E} && \text{(axial in x)} \\
a_{\varphi i} \frac{\partial^2 \varphi_i(x,t)}{\partial t^2} - \frac{\partial^2 \varphi_i(x,t)}{\partial x^2} = 0 \qquad & a_{\varphi ir} = \frac{\rho A_i J_i}{G I_{ti}}, \quad a_{\varphi ic} = \frac{\rho}{G} && \text{(axial around x)}
\end{aligned}
\tag{1}
$$

Applying Bernoulli's method of separation of variables $x(x,t) = X(x)T(t)$ to Eq. (1) and using the approach $W(x) = e^{\lambda x}$, the general solutions for the displacement $W_i(x)$, $V_i(x)$, $U_i(x)$ and $P_i(x)$ for beam i, with $i = 1, \ldots, n$ and C_i, D_i, E_i and F_i as unknown constants, are

$$
\begin{aligned}
W_i(x_i) &= C_{1i} \cos(\lambda_{wi} x_i) + C_{2i} \sin(\lambda_{wi} x_i) + C_{3i} \cosh(\lambda_{wi} x_i) + C_{4i} \sinh(\lambda_{wi} x_i) & \lambda_{wi} &= \sqrt[4]{a_{wi} \omega^2} \\
V_i(x_i) &= D_{1i} \cos(\lambda_{vi} x_i) + D_{2i} \sin(\lambda_{vi} x_i) + D_{3i} \cosh(\lambda_{vi} x_i) + D_{4i} \sinh(\lambda_{vi} x_i) & \lambda_{vi} &= \sqrt[4]{a_{vi} \omega^2} \\
U_i(x_i) &= E_{1i} \cos(\lambda_{ui} x_i) + E_{2i} \sin(\lambda_{ui} x_i) & \lambda_{ui} &= \sqrt{a_{ui} \omega^2} \\
P_i(x_i) &= F_{1i} \cos(\lambda_\pi x_i) + F_{2i} \sin(\lambda_{pi} x_i) & \lambda_{pi} &= \sqrt{a_{\varphi i} \omega^2}.
\end{aligned}
\tag{2}
$$

2.2. Modelling of the transition between segments

In a spatial mechanism the rotation of successive segments about any coordinate axis is possible. However, to achieve the same results, the order of rotation around the axes of the mechanisms is not interchangeable. The x_i-axis points in the direction of the rod axis of the ith segment, and the y_i- and z_i-axes form a cartesian coordinate system for this purpose. The rotating angles between the adjacent segments are in the mathematical positive sense. The transition from segment i to $i+1$ can be described with the matrix in Eq. (3).

This transition is also visualised in Fig. 2. First, it is rotated around the z_i-axis with angle α_i (green). Then around the y_i'-axis with β_i (brown) and finally around x_i'' (corresponding to x_{i+1}) with γ_i (blue). The rotated coordinate system $i + 1$ is shown in blue. This order of rotations corresponds to an intrinsic rotation and is valid for this entire scientific work. The sequence can be realised by multiplying the individual rotation matrices. The corresponding matrix has the following form:

$$
\mathbf{R}_{zyx} = \begin{pmatrix} \cos \alpha_i \cos \beta_i & \cos \alpha_i \sin \beta_i \sin \gamma_i - \sin \alpha_i \cos \gamma_i & \cos \alpha_i \sin \beta_i \cos \gamma_i + \sin \alpha_i \sin \gamma_i \\ \sin \alpha_i \cos \beta_i & \sin \alpha_i \sin \beta_i \sin \gamma_i + \cos \alpha_i \cos \gamma_i & \sin \alpha_i \sin \beta_i \cos \gamma_i - \cos \alpha_i \sin \gamma_i \\ -\sin \beta_i & \cos \beta_i \sin \gamma_i & \cos \beta_i \cos \gamma_i \end{pmatrix}
\tag{3}
$$

From this matrix R_{zyx} a transition matrix for the force and deformation quantities of a spatial mechanism can be constructed.

To describe the transition from segment i to segment $i+1$, the force and deformation quantities are considered while taking into account the following general relations:

$$
\begin{aligned}
N_i &= U_i E A_i & Q_{zi} &= -W_i''' E I_{yi} & M_{byi} &= -W_i'' E I_{yi} \\
Q_{yi} &= -V_i''' E I_{zi} & M_{txi} &= P_i' G I_{Ti} & M_{bzi} &= V_i'' E I_{zi}.
\end{aligned}
\tag{4}
$$

$$
\begin{pmatrix}
N_i \\
Q_{yi} \\
Q_{zi} \\
M_{txi} \\
M_{byi} \\
M_{bzi} \\
U_i \\
V_i \\
W_i \\
P_i \\
-W_i' \\
V_i'
\end{pmatrix}
=
\begin{pmatrix}
R_{zyx} & 0 & \cdots & & 0 \\
0 & R_{zyx} & \cdots & & \vdots \\
0 & \cdots & R_{zyx} & & 0 \\
0 & \cdots & & 0 & R_{zyx}
\end{pmatrix}
\cdot
\begin{pmatrix}
N_{i+1} \\
Q_{yi+1} \\
Q_{zi+1} \\
M_{txi+1} \\
M_{byi+1} \\
M_{bzi+1} \\
U_{i+1} \\
V_{i+1} \\
W_{i+1} \\
P_{i+1} \\
-W_{i+1}' \\
V_{i+1}'
\end{pmatrix}
\tag{5}
$$

$$(12 \times 1) = (12 \times 12) \cdot (12 \times 1)$$

$$\mathbf{I}_i = \mathbf{R}_{3D} \cdot \mathbf{I}_{i+1}$$
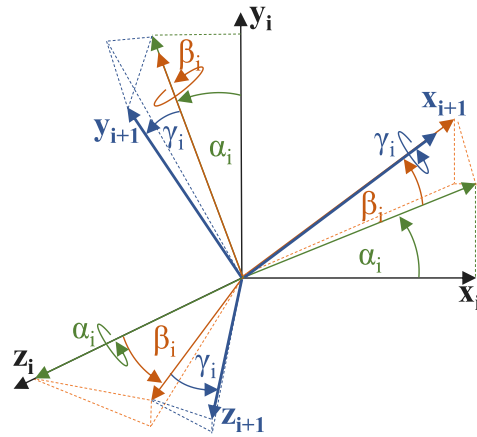
Fig. 2. Spatial coordinate transformation and corresponding matrix vector mulitplication for the transition of the force and deformation quantities from segment i to segment $i+1$.

According to NEWTON's third law, all internal forces and moments must occur in pairs and have the same magnitude with opposite direction of action. If all force quantities are projected onto segment i, the equations Eq. (6) are obtained.

The deformation behaviour at the transition must be continuous and no kinks must occur. The inclination as well as the axial and transverse displacements U, V, W and P are continuous at the transition. The transition conditions are derived in terms of the deformation quantities in Eq. (7).
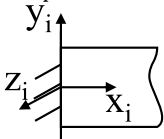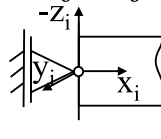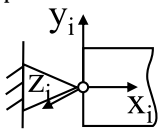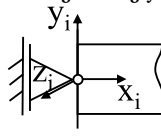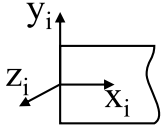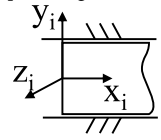
$$
\begin{aligned}
U_i A_i &= U_{i+1} A_{i+1} \cos \alpha_i \cos \beta_i + -V_{i+1}''' I_{zi+1} (\cos \alpha_i \sin \beta_i \sin \gamma_i - \sin \alpha_i \cos \gamma_i) \\
&\quad + -W_{i+1}''' I_{yi+1} (\cos \alpha_i \sin \beta_i \cos \gamma_i + \sin \alpha_i \sin \gamma_i) \\
-V_i''' I_{zi} &= U_{i+1} A_{i+1} \cos \alpha_i \cos \beta_i + -V_{i+1}''' I_{zi+1} (\cos \alpha_i \sin \beta_i \sin \gamma_i - \sin \alpha_i \cos \gamma_i) \\
&\quad + -W_{i+1}''' I_{yi+1} (\cos \alpha_i \sin \beta_i \cos \gamma_i + \sin \alpha_i \sin \gamma_i) \\
-W_i''' I_{yi} &= -U_{i+1} A_{i+1} \sin \beta_i + Q_{yi+1} \cos \beta_i \sin \gamma_i + -W_{i+1}''' I_{yi+1} \cos \beta_i \cos \gamma_i \\
P_i' GI_{Ti} &= P_{i+1}' GI_{Ti+1} \sin \alpha_i \cos \beta_i + -W_{i+1}'' EI_{yi+1} (\cos \alpha_i \sin \beta_i \sin \gamma_i - \sin \alpha_i \cos \gamma_i) \\
&\quad + V_{i+1}'' EI_{zi+1} (\cos \alpha_i \sin \beta_i \cos \gamma_i + \sin \alpha_i \sin \gamma_i) \\
-W_i'' EI_{yi} &= P_{i+1}' GI_{Ti+1} \sin \alpha_i \cos \beta_i + -W_{i+1}'' EI_{yi+1} (\sin \alpha_i \sin \beta_i \sin \gamma_i + \cos \alpha_i \cos \gamma_i) \\
&\quad + V_{i+1}'' EI_{zi+1} (\sin \alpha_i \sin \beta_i \cos \gamma_i - \cos \alpha_i \sin \gamma_i) \\
V_i'' EI_{zi} &= -P_{i+1}' GI_{Ti+1} \sin \beta_i + -W_{i+1}'' EI_{yi+1} \cos \beta_i \sin \gamma_i + V_{i+1}'' EI_{zi+1} \cos \beta_i \cos \gamma_i
\end{aligned}
\tag{6}
$$

$$
\begin{aligned}
U_i(L_i) =& U_{i+1}(0) \cos \alpha_i \cos \beta_i + V_{i+1}(0)(\cos \alpha_i \sin \beta_i \sin \gamma_i - \sin \alpha_i \cos \gamma_i) \\
& + W_{i+1}(0)(\cos \alpha_i \sin \beta_i \cos \gamma_i + \sin \alpha_i \sin \gamma_i) \\
V_i(L_i) =& U_{i+1}(0) \cos \alpha_i \cos \beta_i + V_{i+1}(0)(\cos \alpha_i \sin \beta_i \sin \gamma_i - \sin \alpha_i \cos \gamma_i) \\
& + W_{i+1}(0)(\cos \alpha_i \sin \beta_i \cos \gamma_i + \sin \alpha_i \sin \gamma_i) \\
W_i(L_i) =& - U_{i+1}(0) \sin \beta_i + V_{i+1}(0) \cos \beta_i \sin \gamma_i + W_{i+1}(0) \cos \beta_i \cos \gamma_i \\
P_i(L_i) =& P_{i+1}(0) \sin \alpha_i \cos \beta_i - W'_{i+1}(0)(\cos \alpha_i \sin \beta_i \sin \gamma_i - \sin \alpha_i \cos \gamma_i) \\
& + V'_{i+1}(0)(\cos \alpha_i \sin \beta_i \cos \gamma_i + \sin \alpha_i \sin \gamma_i) \\
-W'_i(L_i) =& P_{i+1}(0) \sin \alpha_i \cos \beta_i - W'_{i+1}(0)(\sin \alpha_i \sin \beta_i \sin \gamma_i + \cos \alpha_i \cos \gamma_i) \\
& + V'_{i+1}(0)(\sin \alpha_i \sin \beta_i \cos \gamma_i - \cos \alpha_i \sin \gamma_i) \\
-V'_i(L_i) =& - P_{i+1}(0) \sin \beta_i + - W'_{i+1}(0) \cos \beta_i \sin \gamma_i + V'_{i+1}(0) \cos \beta_i \cos \gamma_i
\end{aligned}
\tag{7}
$$

2.3. Boundary conditions

The boundary conditions at the beginning and end of the mechanisms, used for solving the differential equations, are summarised in Table 2. The six conditions, clamped, pinned, free, floating bearing z and y and parallel guide are considered.

Table 2
Boundary conditions, beginning and end.

Boundary condition	Beginning $x_1 = 0$	End $x_n = L_n$		Boundary condition	Beginning $x_1 = 0$	End $x_n = L_n$	
clamped	$U_1(0) = 0$	$U_n(L_n) = 0$		**floating bearing z**	$U_1(0) = 0$	$U_n(L_n) = 0$	
	$V_1(0) = 0$	$V_n(L_n) = 0$			$V_1(0) = 0$	$V_n(L_n) = 0$	
	$W_1(0) = 0$	$W_n(L_n) = 0$	(8a)		$P'_1(0) = 0$	$P'_n(L_n) = 0$	(8d)
	$P_1(0) = 0$	$P_n(L_n) = 0$			$V''_1(0) = 0$	$V''_n(L_n) = 0$	
	$V'_1(0) = 0$	$V'_n(L_n) = 0$			$W''_1(0) = 0$	$W''_n(L_n) = 0$	
	$W'_1(0) = 0$	$W'_n(L_n) = 0$			$W'''_1(0) = 0$	$W'''_n(L_n) = 0$	
pinned	$U_1(0) = 0$	$U_n(L_n) = 0$		**floating bearing y**	$U_1(0) = 0$	$U_n(L_n) = 0$	
	$V_1(0) = 0$	$V_n(L_n) = 0$			$W_1(0) = 0$	$W_n(L_n) = 0$	
	$W_1(0) = 0$	$W_n(L_n) = 0$	(8b)		$P'_1(0) = 0$	$P'_n(L_n) = 0$	(8e)
	$P'_1(0) = 0$	$P'_n(L_n) = 0$			$V''_1(0) = 0$	$V''_n(L_n) = 0$	
	$V''_1(0) = 0$	$V''_n(L_n) = 0$			$W''_1(0) = 0$	$W''_n(L_n) = 0$	
	$W''_1(0) = 0$	$W''_n(L_n) = 0$			$V'''_1(0) = 0$	$V'''_n(L_n) = 0$	
free	$U'_1(0) = 0$	$U'_n(L_n) = 0$		**parallel guide**	$U_1(0) = 0$	$U_n(L_n) = 0$	
	$P'_1(0) = 0$	$P'_n(L_n) = 0$			$V_1(0) = 0$	$V_n(L_n) = 0$	
	$V''_1(0) = 0$	$V''_n(L_n) = 0$	(8c)		$W_1(0) = 0$	$W_n(L_n) = 0$	(8f)
	$V'''_1(0) = 0$	$V'''_n(L_n) = 0$			$U'_1(0) = 0$	$U'_n(L_n) = 0$	
	$W''_1(0) = 0$	$W''_n(L_n) = 0$			$V'_1(0) = 0$	$V'_n(L_n) = 0$	
	$W'''_1(0) = 0$	$W'''_n(L_n) = 0$			$W'_1(0) = 0$	$W'_n(L_n) = 0$	

2.4. Analytical model

The equations derived from the EULER–BERNOULLI-Beam theory, see Eq. (2), solved with the boundary and transition conditions, Eqs. (8a)–(8f), (see Table 2), (6) and (7), lead to a system of equations. Solving this system for the constants C_i, D_i, E_i, and F_i, with $i = 1, \ldots, n$ and n representing the number of segments of the mechanism, it can be written as a coefficient matrix notation as follows.

$$
\begin{pmatrix}
x_{1,1} & x_{2,1} & \cdots & x_{a-1,1} & x_{a,1} \\
x_{1,2} & x_{2,2} & \cdots & x_{a-1,2} & x_{a,2} \\
\vdots & \vdots & \ddots & \vdots & \vdots \\
x_{1,b-1} & x_{2,b-1} & \cdots & x_{a-1,b-1} & x_{a,b-1} \\
x_{1,b} & x_{2,b} & \cdots & x_{a-1,b} & x_{a,b}
\end{pmatrix}
\cdot
\begin{pmatrix}
C_{1(i)} \\
C_{2(i)} \\
\vdots \\
F_{1(i)} \\
F_{2(i)}
\end{pmatrix}
=
\begin{pmatrix}
0 \\
0 \\
\vdots \\
0 \\
0
\end{pmatrix}
\tag{9}
$$

$$\mathbf{T} \cdot \mathbf{K} = \mathbf{0}$$

The constants C_i, D_i, E_i, and F_i are summarised in the vector $\mathbf{K}$ (size $12nx1$). The matrix $\mathbf{T}$ (size $12nx12n$) is the coefficient matrix, whose non-trivial solutions are the natural frequencies of the considered compliant systems. In order to calculate these non-trivial solutions the frequencies ω are searched, for which the determinant of $\mathbf{T}$ is equal to 0. These frequencies are the natural frequencies of the mechanism.
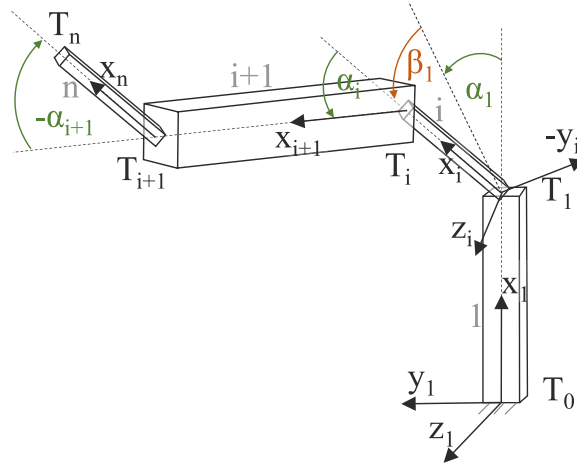
Fig. 3. Model of a spatial compliant mechanism with 4 segments, segment i to segment 1 is rotated according to Eq. (3) around the x_1- and around the $y\prime_1$-axis.

In general, to solve the differential equations of a single segment, 6 boundary conditions are needed for the beginning and 6 for the end. For each additional segment, 12 additional transition conditions are added to the system of equations. Accordingly, the matrix **T** becomes larger by 12 rows and columns with each additional segment. Already for three segments, **T** is a 36×36 matrix. Computing the determinant of matrices of this size quickly exceeds the computational capacity of commonly used computers.

In order to be able to perform the calculation faster and for arbitrarily large compliant mechanisms, see Fig. 3 for example, individual matrices and systems of equations can be set up for the beginning, the transitions and the end of the respective mechanism.

Instead of the global matrix **T**, the mechanism is split into the individual matrices $\mathbf{T}_0$ (size $12x6$), $\mathbf{T}_i$ (size $12x12$) and $\mathbf{T}_n$ (size $6x12$) see Eq. (10), for $i = 1, \ldots, n_{-1}$. These are in turn interdependent.

$$\text{end} \qquad\qquad \mathbf{T}_n \mathbf{K}_n = \mathbf{0} \qquad\qquad\qquad (10a)$$

$$\text{transition} \qquad \begin{aligned} \mathbf{T}_{iL}\mathbf{K}_i &= \mathbf{T}_{i+1R}\mathbf{K}_{i+1} \\ \mathbf{T}_{i+1R}^{-1}\mathbf{T}_{iL}\mathbf{K}_i &= \mathbf{K}_{i+1} \\ \mathbf{T}_i \mathbf{K}_i &= \mathbf{K}_{i+1} \qquad (\mathbf{T}_1 \mathbf{K}_1 = \mathbf{K}_i) \end{aligned} \qquad (10b)$$

$$\text{beginning} \qquad\qquad \mathbf{T}_0 \mathbf{K}_0 = \mathbf{K}_1 \qquad\qquad\qquad (10c)$$

Eq. (10c), n times Eq. (10b) and Eq. (10a) can then be substituted. The output of the ith segment is the input of the $i+1$th and so on. This results in the following equation:

$$\begin{aligned} \mathbf{T}_n \mathbf{T}_{n-1} \cdots \mathbf{T}_{i+1}\mathbf{T}_i\mathbf{T}_1\mathbf{T}_0\mathbf{K}_0 &= \mathbf{0} \\ \rightarrow \mathbf{TK}_0 &= \mathbf{0} \end{aligned} \qquad (11)$$

The natural frequencies of the mechanism result from the nontrivial solutions of the transfer matrix **T**, which has always the size $6x6$, therefore

$$det(\mathbf{T}) = 0. \qquad\qquad\qquad (12)$$

Eqs. (11), (12) and all formulas on which these are based form the basis for the developed calculation tool.

2.5. Flexure hinge

The compliant segments, or flexure hinges, of compliant mechanisms often have a different contour than simple straight beam or bar segments. Among the most common joint contours are the semicircular contour, the quarter-circular contour, the elliptical contour and the polynomial contour of different order [23,24]. For the calculation tool, the calculation of flexure hinges with semicircular contour is derived.

In order to describe the semicircular contour of the flexure hinge with the elaborated analytical model, one possible approach is to divide it into n segments, as shown in brown in Fig. 4. Combining these segments, they can be seen as a planar mechanism where all angles are 0. For the transitions, each force and deformation element is equal to that of the predecessor: $N_i = N_{i+1}$ etc. It is assumed that the width is constant over the entire solid joint and, in this work, that the length of the semicircular contours
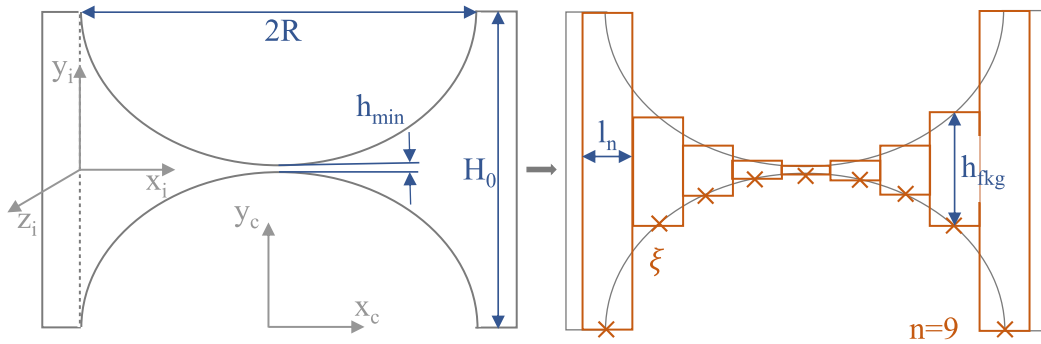
Fig. 4. Approximation of a semicircular flexure hinge via, for example, 9 rectangular segments.

is equal to $L = 2R$, where R is the radius of the semicircular contour. Furthermore, it is specified that all segments have the same length and can be calculated using Eq. (13).

$$l_n = \frac{2R}{n} \tag{13}$$

To calculate the height h_{fkg} of the individual segments, it is necessary to describe the semicircular contour approximately. From the circle equation in normal form $x_c^2 + y_c^2 = R^2$ the following function is obtained. It represents a semicircular contour opened downwards.

$$y_c(x) = \sqrt{R^2 - x_c^2} \quad \text{for} -R \le x_c \le R \tag{14}$$

Certain coordinates of the extreme fibre $y(x)$ are called support points ξ. They represent the centre of each segment length and are shown as brown crosses in Fig. 4. Their position depends on the segment length l_n and thus on their total number n. They are used to calculate the heights $h_{fkg,i}$ of each individual segment, see Eq. (16).

$$\xi_i = \frac{l_n}{2} + (i+1)l_n; \quad i = 1, \ldots, n \tag{15}$$

$$h_{fkg,i} = 2R + h_{min} - 2\sqrt{R^2 - (\xi_i - R)^2} \tag{16}$$

Finally, the minimum number of segments necessary to correctly approximate the semicircular flexure hinge was derived. For this purpose, the first natural frequency of several flexure hinges are calculated for $n = 1, \ldots, 100$ and illustrated as can be seen in Fig. 5. The function strives for a limit value at a segment number of 25, meaning, that the approximation of the semicircular flexure hinge is sufficiently accurate for at least 25 segments.
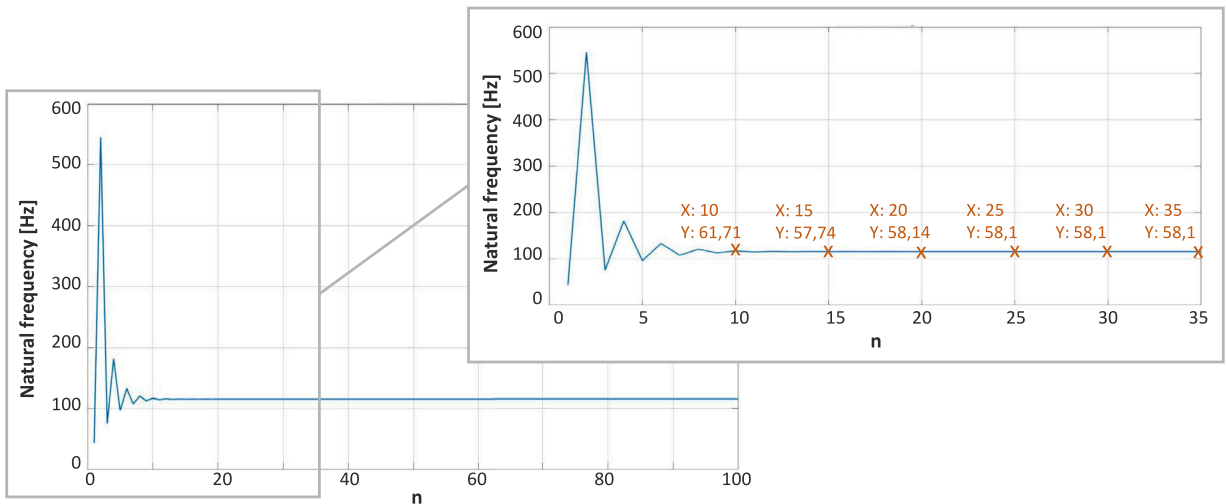

Fig. 5. Limit value determination of semicircular flexure hinge for $n = 1 - 100$, close-up for $n = 35$.

3. Program implementation

The method for calculating the natural frequencies of serial compliant mechanisms as described above can be easily implemented into a graphical user interface due to consistent calculation of the matrices and the pre defined boundary conditions. The segments
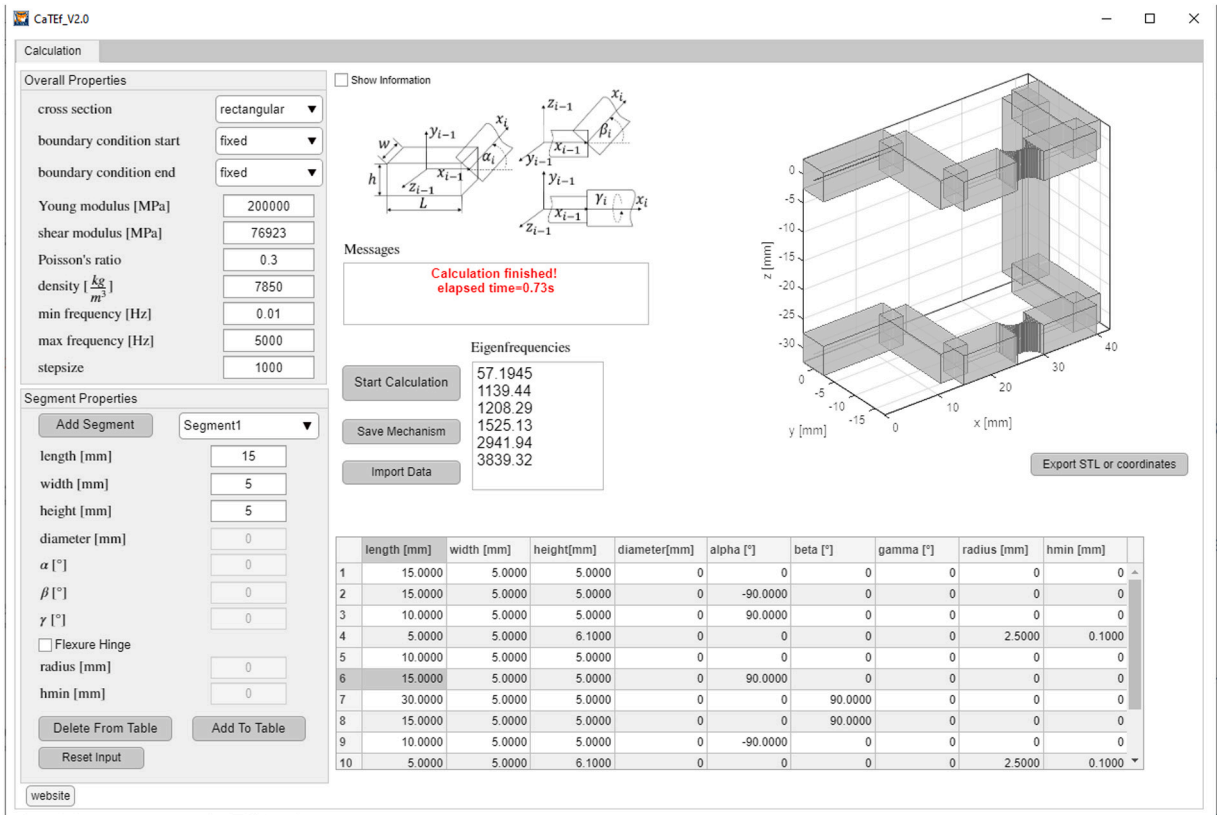
Fig. 6. Screenshot of the developed GUI.

of the mechanism are constructed individually with a constant circular or rectangular cross-section or with a semicircular flexure hinge contour. Assigning geometric parameters to each segment like length, transition angles, height, width or radii allows to create a continuous compliant mechanism. The six different boundary conditions are pre defined and can be selected and the frequency range can be chosen freely as well as the calculation step size. The presented graphical user interface, see Fig. 6, is developed using the GUIDE environment in MATLAB.

3.1. Mathematical implementation

The analytical model from Section 2.4 and especially Eqs. (11) and (12) are the basis of the developed calculation program. The calculation of the natural frequencies, as well as all boundary and transition conditions and the necessary matrix multiplications are stored in MATLAB scripts as individual functions. The graphical user interface is used to enter and/or select the parameters necessary for the calculation. These are then passed to the function(s) through which the calculation is performed. The results are returned and displayed in the graphical user interface. In very general terms, a function graph of the determinants $D(\omega)$ of $\mathbf{T}$ for a specified ω range, see Eq. (17), is generated, whose zero crossings represent the natural frequencies of the mechanism.

$$D(\omega) = det(\mathbf{T}(\omega)) \tag{17}$$

The matrix $\mathbf{T}$ results from the boundary and transition conditions. The boundary conditions are the initial and final conditions of the mechanism and are selected via the user interface. Each six possible boundary conditions are stored in a separate if-elseif structure which selects the desired matrix by comparison of string. These are then saved as the start condition matrix $\mathbf{T}_0$ and the end condition matrix $\mathbf{T}_n$.

The number of segments determines the number of transition conditions and thus transition matrices $\mathbf{T}_i$, see Eq. (10b). The appropriate values for each transition ($\rho, E, G, L_i, L_{i+1}, h_i, h_{i+1}, b_i, b_{i+1}, d_i, d_{i+1}, \alpha_i, \beta_i, \gamma_i$) are passed to the integrated function for the calculation of the transition matrices. Element by element, the corresponding cross-sections and moments of inertia are calculated, and based on that, the corresponding transition matrices.

$\mathbf{T}_0$, n-1 $\cdot\mathbf{T}_i$ and $\mathbf{T}_n$ are then multiplied, see Eq. (11), and the determinants are calculated as a function of ω, see Eq. (17). The range for ω is previously entered in the user interface by the user. The MATLAB function *fzero* is then used to find the values of the function $D(\omega)$ for which a sign change occurs and, accordingly, where the function has a zero. These values are the natural angular frequencies of the mechanism, but the output occurs as the natural frequencies.
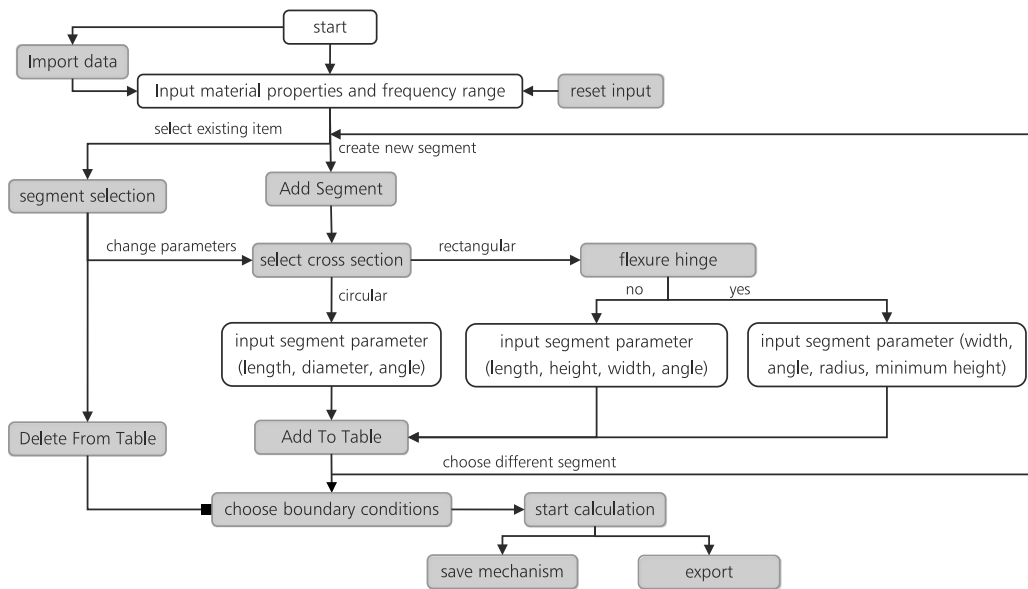
Fig. 7. Visual representation of the program structure.

3.2. Program structure of the graphical user interface

The developed GUI is shown in Fig. 6. The interface is structured into three main modules: the *input*, the *output* and the *visual representation*. The *input* consists of the input of the overall properties, like boundary conditions, material parameters and frequency range and can be found at the upper left side. It also includes the input of the individual segment parameters, at the bottom left, as well as the reading in of pre-stored data. The message- and result textbox as well as the export button belong to the *output* of the program. The *visual representation* consist of the display of the segment parameters at the top of the interface and the rod axis of the segments are shown as lines in a three dimensional coordinate system at the right side.

A flow chart of the implemented modules is given in Fig. 7. The desired cross-sections, circular or rectangular, are selected segment by segment via the *cross section* selection menu. For the latter, it is additionally possible to add a semicircular solid hinge, see Section 2.5 to the mechanism via the *flexure hinge* checkbox. Once the segment parameters have been entered, they are added to the table via the *add to table* button. Using the *choose segment* drop-down menu, segments can be selected from the table again and their values read in. Selected segments are highlighted in black in the display for better understanding. The segment can then either be adjusted or deleted using the *delete from table* button. The *reset input* button deletes all data from the table and the structural representation. The *start calculation* button starts the calculation. The results are then displayed in the *eigenfrequencies* field. These, along with all parameters of the mechanism, can be exported via the *save mechanism* button to a excel or text file for further processing by other software.

4. Validation and verification

Following, compliant mechanism examples are investigated using the developed software CaTEf. First, the results are compared to FEM simulations conducted in ANSYS WORKBENCH and to measurements from previous investigations [5,6,17] and afterwards, further mechanisms, spatial and planar, are compared to FEM and an experiment is carried out for validation. Example mechanisms are illustrated in Fig. 8. Finally an experiment is carried out, to verify the Tool for real life applications.

The element type used in the FEM simulations in ANSYS WORKBENCH is PLANE183. A modal analysis was carried out and the models were either build in DesingModeler in ANSYS or imported from a CAD-model. In order to obtain meaningful results, the meshing of the segments was varied. It was distinguished between the area of the flexure hinges and all other segments. With smaller element sizes, the result for the total deformation changed minimally, but the calculation time became significantly longer as a result, especially for the area of the flexure hinges. Therefore, these sections were meshed over a radius of 3 mm with an element size of 0.05 mm. The sections of the other segments were meshed with an element size of 0.5 mm.

4.1. Comparison with previous studies

For a first verification, two example compliant mechanisms from previous studies are considered and replicated to compare the results obtained using CaTEf and the respective approaches with the FEM results and then with each other. Both mechanisms
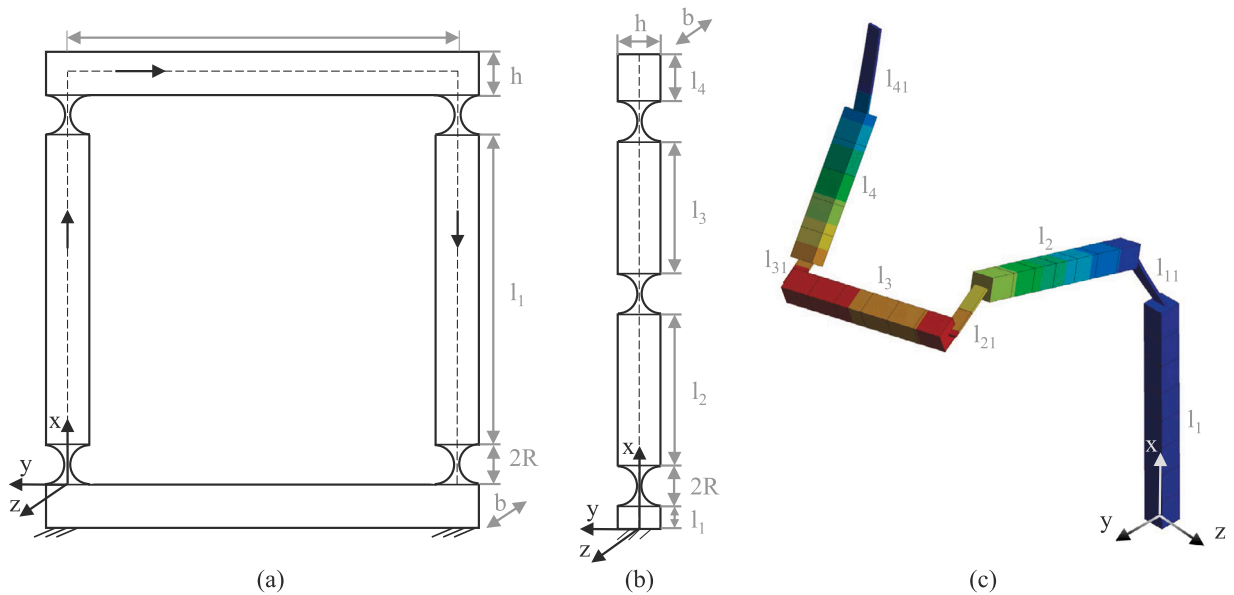
Fig. 8. (a) Parallel-guided compliant mechanism with semicircular flexure hinges from [5,6], with $l_1 = 24$, $l_2 = 36.6$, $R = 3$, $h_{min} = 0.6$, $h = 6.6$ and $b = 8$ in [mm], fixed fixed, (b) Planar serial compliant mechanism with semicircular flexure hinges from [17], with $l_1 = 7.5$, $l_2 = 35$, $l_3 = 35$, $l_4 = 17.5$, $R = 5$, $h_{min} = 1$, $h = 11$ and $b = 10$ in [mm], fixed free, (c) Spatial compliant mechanism with distributed compliance, with $l_1 = 85$, $l_{11} = l_{41} = 30$, $l_2 = 80$, $l_{21} = 20$, $l_3 = 60$, $l_{31} = 10$, $l_4 = 50$, $R = 5$, $h_{min} = 1$, $h = b = 8$ and $h_s = 5$, $b_s = 1$ in [mm], $\alpha_1 = 30$, $\alpha_2 = \alpha_3 = 45$, $\alpha_6 = -30$, $\alpha_7 = -20$, $\beta_4 = \beta_5 = 90$ in [°], fixed fixed.

are planar and have concentrated compliance in the form of semicircular flexure hinges. The parallel-guided compliant mechanism from [6] and the planar serial flexure hinge-based compliant mechanisms from [17] are shown in Fig. 8.

The boundary conditions at the beginning and end of the parallel-guided compliant mechanism are both fixed. The results for the natural frequencies are given in Table 3.

Table 3
Verification of the CaTEf-results on the example of the parallel-guided compliant mechanism from [5,6], see Fig. 8(a), Δ-deviation to FEM results, NF-natural frequency.

Method	1st NF in Hz	Δ in %	2nd NF in Hz	Δ in %	3rd NF in Hz	Δ in %
3D FEM	288.00	–	1385.00	–	2635.00	–
CaTEf	288.16	+0.06	1514.26	+9.33	2780.00	+5.5
[5]	287.70	−0.10	–	–	–	–
[6]	273.00	−5.21	1312.00	−5.27	2379.00	−9.72

Table 4 presents the results for the natural frequencies of the serial compliant mechanism, whose boundary condition at the beginning is also fixed and whose end is free. It can be seen that the analytical method from this work provides very good agreement with the results from ANSYS and the previous calculations. The results for the first natural frequency have especially good correlation.

Table 4
Verification of the CaTEf-results on the example of the planar serial flexure hinge-based compliant mechanism from [17], see Fig. 8(b), Δ-deviation to FEM results, NF-natural frequency.

Method	1st NF in Hz	Δ in %	2nd NF in Hz	Δ in %	3rd NF in Hz	Δ in %
3D FEM	62.28	–	350.87	–	418.15	
CaTEf	62.60	0.52	375.26	6.95	424.84	1.60
[17]	65.05	4.45	–	–	–	–

4.2. Validation with numerous mechanisms

Numerous mechanisms, planar and spatial, have been investigated and their results were compared to 3D FEM results to further verify the proposed analytical method and its implementation in the calculation tool CaTEf. They are classified according to their compliance — distributed, concentrated and in form of semicircular flexure hinges.

The deviations of the results for the first natural frequency, independently of their compliance — are overall very small. Furthermore, for mechanisms with distributed compliance most results obtained with CaTEf are in very good correlation with the results from FEM ($\leq 5\%$), as exemplarily shown in Table 5 for the spatial compliant mechanism in Fig. 8(c).

Table 5

Verification of the CaTEf-results on the example of a spatial compliant mechanism see Fig. 8(c), Δ-deviation to FEM results, NF-natural frequency in Hz, Young's modulus=200.000 MPa, density=7850 $\frac{kg}{m^3}$.

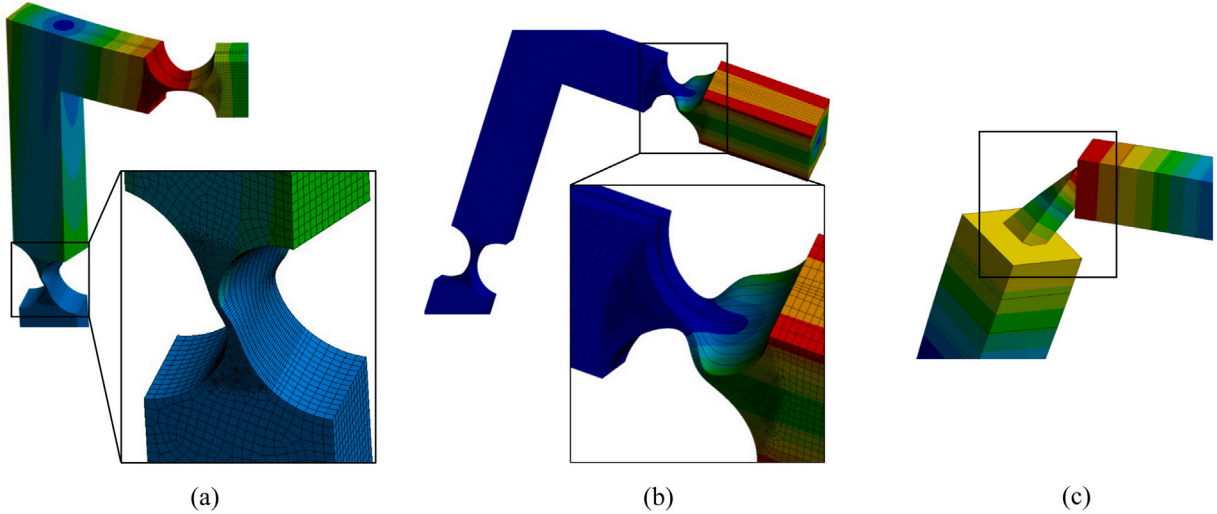|	1st NF in Hz	2nd NF in Hz	3rd NF in Hz	4th NF in Hz	5th NF in Hz	6th NF in Hz	7th NF in Hz	8th NF in Hz
CaTEf	51,90	75,31	156,94	196,40	344,27	508,48	570,67	836,58
FEM	52,11	75,86	157,15	196,21	343,13	505,26	567,09	831,20
Δ in %	−0,39	−0,73	−0,14	0,10	0,33	0,64	0,63	0,65

Fig. 9. Deformation of the compliant segments (a) and (b) semicircular flexure hinge (c) rectangular cross-section.

Comparatively larger deviations, up to 10%, can be found for mechanisms with rectangular cross-sections. The results for mechanisms with concentrated compliance are also in good correlation with the FEM results. Deviations higher than 10% occur only for spatial mechanisms with more than five segments and rectangular cross-sections, and for mechanisms with the boundary conditions clamped and floating bearing z, see Eqs. (8a) and (8d).

The results for mechanisms which are flexure-hinge based, show more natural frequencies with higher deviations to the FEM results, than the other compliant mechanisms. It can be generally seen that especially for natural frequencies where the solid joints are twisted, i.e. torsion flows proportionally or completely into the motion, or a motion in the direction of their z-axis takes place, the deviations are very high (over 50%). Using examples, this relationship is illustrated in Fig. 9.

4.3. Discussion of the analytical results

The high deviations of these natural frequencies are due to various causes. The analytical model developed in this work is based on the BERNOULLI beam theory. This means, that shear deformation and occurring cross-sectional warping are neglected. This approximation is not admissible, especially for large deformations. A closer look at the individual vibration modes of the mechanisms where larger deviations can be found reveals that they occur for the natural frequencies, where large deformations at the compliant segments can be seen, see Fig. 9. Moreover, the beam theory is valid only for slender beams. This explains the higher deviations occurring for mechanisms with short (concentrated) compliant segments. Furthermore, the highest deviations occur for mechanisms with rectangular cross-sections. These are due to the neglected cross-section warping and to the approximation of the torsional moment of inertia for rectangular and square cross-sections, see Eq. (18), which is only an approximation and the calculation is accordingly inaccurate.

$$\text{rectangular cross-section} \quad I_t = cbh^3 \quad \text{with} \quad c = \frac{1}{3}\left(1 - \frac{0.63}{h/b} + \frac{0.052}{(h/b)^5}\right) \quad [25]$$

$$\text{circular cross-section} \quad I_p = \frac{\pi d^4}{32} \quad \text{(see Fig. 10 and Table 6 for parameter reference)}$$

(18)

When modeling the semicircular solid joints, the affected section is divided into n narrow disk-like segments, see Section 2.5. The term slender beam is not correct for these segments. Due to the compactness of the solid joints, the neglect of shear and the cross-sectional buckling is apparently inadmissible, when considering rotational movements. Accordingly, the underlying BERNOULLI beam theory is inadequate.

4.4. Validation through experiment

To validate the analytical model, the natural frequencies of three parallel-guided compliant mechanisms with four semicircular solid joints were measured. The frequencies were then compared with the analytically calculated values and the calculated values of an FEM model in ANSYS Workbench 2020 R2.

4.4.1. Experimental setup

The basis of the experiment carried out is the non-contact measurement of the free vibrations of the test specimens. It is based on the experiments from [26], as is the experimental procedure. The test specimens are made of a high-strength aluminum alloy EN AW-7021 C330R. The material and geometry parameters are listed in the following Fig. 10 and Table 6.
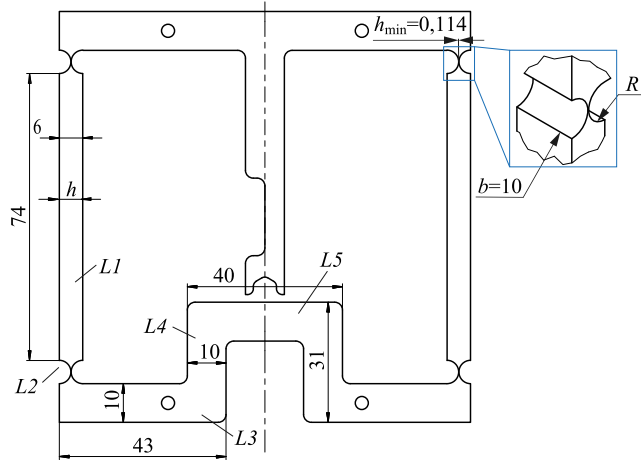

Fig. 10. Dimensions of the parallel-guided compliant mechanism.

Table 6

Parameters of the parallel-guided compliant mechanisms.

Parameter	Symbol	Value	Unit
Young's modulus	E	70000	MPa
Poisson's ratio	v	0.33	
Density	ρ	2800	$\frac{kg}{m^3}$
width	b	10	mm
height	h	6/10	mm
minimal height	h_{min}	0.144	mm
radius	R	3	mm

The natural frequency was determined using the setup shown in Fig. 11. The chromatic-confocal distance sensor Micro-Epsilon – IFS2405-0,3 is mounted on a motorised linear guide in the y-direction. With the help of the linear guide in x-direction, the test specimen are finely positioned manually in the measuring range of the sensor. Due to the very delicate notch height of the flexure hinges, the mechanisms are excited only by hand. The deflection is then measured over time and from the resulting diagram, an amplitude and frequency curve is determined via the fast Fourier transformation. For each test specimen, the measurement was performed five times for 100 s each with a sampling rate of 1 kHz. This results in a frequency resolution of the fast Fourier transform of 0.01 Hz. The standard deviation was neglected because it was below the frequency resolution.

In Fig. 12, the amplitude over frequency curves are summarised for each individual specimen for all five performed measurements in one graph per specimen. The first natural frequency is clearly visible at the point of highest amplitude. The experiments resulted in the following natural frequencies of the three specimens: PC1 = 6.06 Hz, PC2 = 6.03 Hz, PC3 = 6.01 Hz with the mean value of $\bar{PC} = 6.03\overline{3}$ Hz.

4.4.2. Calculation in catef and ANSYS

In order to obtain meaningful results in ANSYS, the meshing was varied in the area of the flexure hinges, see Table 9 in the appendix. With smaller element sizes, the result for the total deformation changed minimally, but the calculation time became significantly longer as a result. The sections of the flexure hinges were meshed over a radius of 3 mm with an element size of 0.05 mm. The calculated results of the natural frequencies in ANSYS for the mechanisms with and without holes are: with holes NF= 6.308 Hz   without holes NF_{no} = 6.276 Hz.

According to [26], previous experiments with similar models show that the natural frequencies differ, when comparing the measured results to the results obtained with a model using the ideal geometry (as are the calculations in ANSYS and CaTEf). These discrepancies suggest inaccuracies in the geometry in the relevant region, the minimum height h_{min} of the flexure hinges. This will
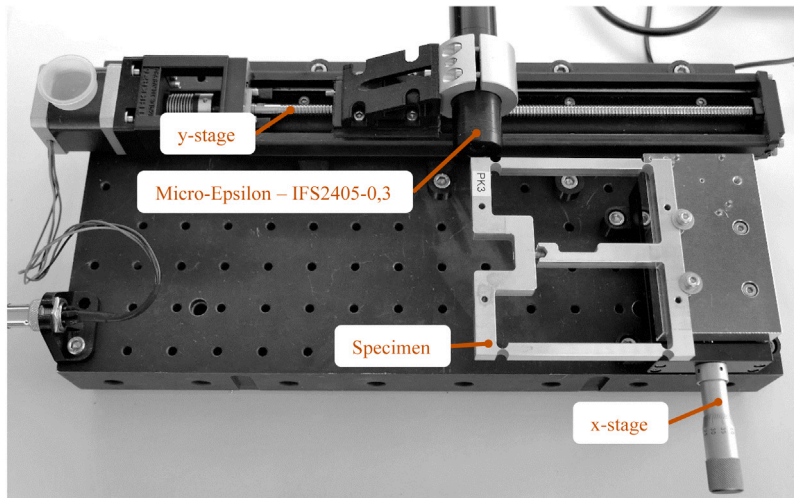
Fig. 11. Experimental setup for determination of the first natural frequency of a parallel-guided compliant mechanism with semicircular flexure hinges.
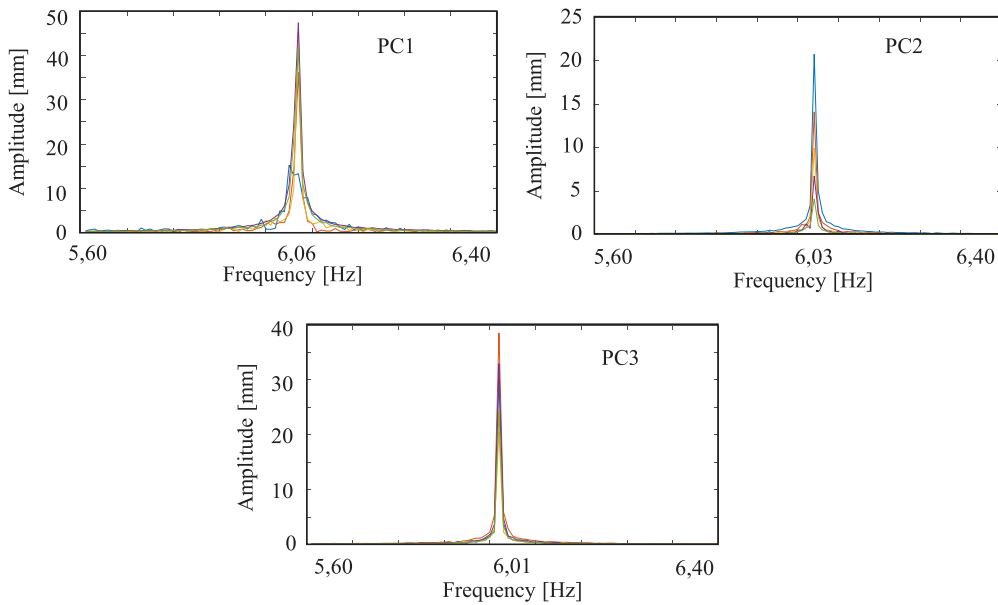

Fig. 12. Frequency spectrum of the five performed measurements for each of the specimen PC1, PC2 and PC3.

Table 7
Variation of the minimum height h_{min} in CaTEf and resulting deviations from the measured results.

h_{min} in mm	NF (CaTEf) in Hz	NF (Experiment) in Hz	Δ in %
0.1100	5.9806		−0.87
0.1105	6.0147		−0.30
0.1110	**6.0488**		**+0.26**
0.1120	6.1171	$6.0\overline{33}$	+1.39
0.1130	6.1855		+2.53
0.1140	6.2541		+3.66

be discussed further at the end of this section. Based on these assumptions, several calculations are performed in CaTEf, in which h_{min} is varied, Table 7.

This study shows, that the dimension of the flexure hinges has great influence on the overall dynamic performance of the mechanisms. Merely 3 μ m difference at the minimal notch height result in a 3% difference of the natural frequency.

4.4.3. Discussion of the experimental results

As shown in Table 7, with an h_{min} of 114 μm, the deviation of the value calculated by CaTEf from the measured comparison value is +3.66%.

As mentioned above, such a deviation was already observed in previous experiments in [26]. It suggests that material is missing from the relevant zone (h_{min}) in the flexure hinges — it is smaller than specified in the manufacturing template. This is due to various causes. On the one hand, the dimension of h_{min} may deviate due to manufacturing tolerances, on the other hand, it may deviate due to waviness and roughness of the surface or due to changes in the surface properties. It was not possible to determine the actual h_{min} for further prove of this theory.

Another possible reason for the deviation of the measured and calculated results are the missing holes in the model of the calculation tool. The parallel-guided compliant mechanism is calculated in CaTEf without holes. It is not possible to include them in the model, but the lower density at their place can be represented by a reduction in the cross-section. For this purpose the $L3$ segment, see Fig. 10, was divided into three segments and the height of the middle part was reduced. Two different approaches for the reduction were used. In the first approach, the middle segment was replaced by a semicircular flexure hinge. In the second approach, the middle segment remained a beam segment, but its height was reduced. For better comparison, the calculations in ANSYS WORKBENCH were carried out both with and without the holes. The studies show that the second approach provides the better results, see Table 8.

Table 8
Results of CaTEf and ANSYS without and with holes. Approximation of the holes in CaTEf through (a) a smaller beam segment and (b) a flexure hinge in comparison to the ANSYS results.

Mechanism	Small segment	In mm	in Hz	ANSYS in Hz	Δ_{ANSYS} in %
No holes		10.0	6.2541	6.276	−0.35
(a)	h	6.0	6.3239		+0.25
		7.0	6.3063		−0.03
		8.0	6.2888	6.0308	−0.30
(b)	h_{min}	4.0	6.3949		+1.38
		4.5	6.3781		+1.11
		4.7	6.3715		+1.01

It can also be clearly seen that the holes have no influence on the deviations of the natural frequencies from experiment to calculation that occurred here. Due to the reduction of the cross-section in the relevant area, the natural frequency increases in the calculation instead of reclining. Therefore the deviations can be attributed to the inaccuracy in the minimum height of the flexure hinges.

Nevertheless, the deviations are comparably small and the studies have shown, that the analytical model and the resulting calculation tool CaTEf are suitable to extend or even replace real experiments. The results show good agreement. Comparing the results obtained with CaTEf with the results from ANSYS, it enables an almost exact calculation of ideal geometries.

5. Conclusions

With this contribution, the authors presented an analytical model and algorithm, which enables the fast and uncomplex calculation of the natural frequencies of compliant mechanisms. It can be used, for example, in the design phase to prevent harmonic reactions or to troubleshoot when existing machines show signs of harmonic interaction. The model and algorithm have been implemented into an intuitive MATLAB-based graphical user interface. It is applicable for serial spatial compliant mechanisms with varying cross-sections, boundary conditions and material properties. To the authors knowledge, no previous tools have been designed for the calculation of the natural frequencies of spatial compliant mechanism. The greatest advantage over the previous works presented in Table 1 and FEM is the adaptability, the fast design and the calculation time of the presented tool. With CaTEf the design of compliant mechanisms like the examples in Figs. 8 and 10 can be accomplished by simply adding elements with the desired parameters. The calculation of the natural frequencies is therefore vastly accelerated and can be achieved in a matter of seconds. Another advantage is the export and import option of the tool, which allows to re-read pre-saved data, so that similar mechanisms can be modified and do not have to be build from scratch. The analytical solution has been verified by means of FEM simulations and validated through an experiment. As observed in the experiment, compliant mechanisms are very sensible to manufacturing tolerances, especially the flexure hinges. Therefore CaTEf can be used to simulate the consequences deriving from manufacturing variations. It was noted, that the approximation of the flexure hinges as a set of BERNOULLI-Beams is somewhat inaccurate and will be subject to future research, the same applies for the accuracy of torsional movements. For increase of range of application the implementation of branching points will also be further researched. A download link to the software can be provided upon request to the corresponding author.

Declaration of competing interest

The authors declare that they have no known competing financial interests or personal relationships that could have appeared to influence the work reported in this paper.

Appendix A

See Fig. 13 and Table 9.

Table 9
Natural frequencies (NF) of the parallel-guided compliant mechanisms for different element sizes (ES) of the flexure hinge in ANSYS.

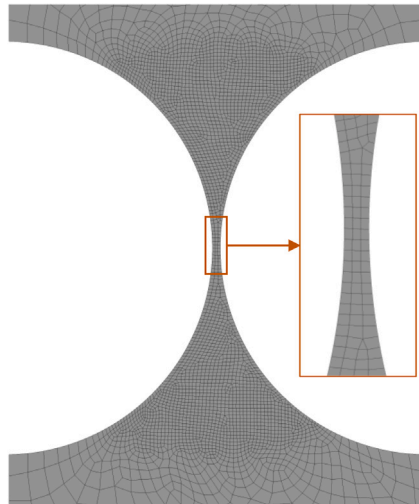| ES in mm	NF of mech. in Hz	
	With holes	Without holes
0.5	6.351	6.139
0.1	6.311	6.279
0.05	6.308	6.276
0.04	6.308	6.276
0.03	6.308	6.276

Fig. 13. Element size of the flexure hinge of the parallel-guided compliant mechanism.

Appendix B. Supplementary data

Supplementary material related to this article can be found online at https://doi.org/10.1016/j.mechmachtheory.2022.104939.

References

[1] L.L. Howell, S.P. Magleby, B.M. Olsen (Eds.), Handbook of Compliant Mechanisms, John Wiley & Sons Inc, Chichester West Sussex United Kingdom and Hoboken, 2013.

[2] S. Henning, L. Zentner, Analysis of planar compliant mechanisms based on non-linear analytical modeling including shear and lateral contraction, Mech. Mach. Theory (164) (2021) http://dx.doi.org/10.1016/j.mechmachtheory.2021.104397.

[3] V. Megaro, J. Zehnder, M. Bächer, S. Coros, M. Gross, B. Thomaszewski, A computational design tool for compliant mechanisms, ACM Trans. Graph. 36 (4) (2017) 1–12, http://dx.doi.org/10.1145/3072959.3073636.

[4] J.B. Jonker, J.P. Meijaard, SPACAR — Computer program for dynamic analysis of flexible spatial mechanisms and manipulators, in: W. Schiehlen (Ed.), Multibody Systems Handbook, Springer Berlin Heidelberg, Berlin, Heidelberg, 1990, pp. 123–143, http://dx.doi.org/10.1007/978-3-642-50995-7_9.

[5] M. Ling, J. Cao, Z. Jiang, J. Lin, A semi-analytical modeling method for the static and dynamic analysis of complex compliant mechanism, Precis. Eng. 52 (2018) 64–72, http://dx.doi.org/10.1016/j.precisioneng.2017.11.008.

[6] Y. Shen, X. Chen, W. Jiang, X. Luo, Spatial force-based non-prismatic beam element for static and dynamic analyses of circular flexure hinges in compliant mechanisms, Precis. Eng. 38 (2) (2014) 311–320, http://dx.doi.org/10.1016/j.precisioneng.2013.11.001.

[7] Z. Li, S. Kota, Dynamic analysis of compliant mechanisms, in: L.L. Howell (Ed.), Proceedings of the 2002 ASME Design Engineering Technical Conferences and Computers and Information in Engineering Conference, American Society of Mechanical Engineers, New York, NY, 2002, pp. 43–50, http://dx.doi.org/10.1115/DETC2002/MECH-34205.

[8] W. Wang, Y. Yu, Analysis of frequency characteristics of compliant mechanisms, Front. Mech. Eng. China 2 (3) (2007) 267–271, http://dx.doi.org/10.1007/s11465-007-0046-2.

[9] M. Rösner, R. Lammering, R. Friedrich, Dynamic modeling and model order reduction of compliant mechanisms, Precis. Eng. 42 (2015) 85–92, http://dx.doi.org/10.1016/j.precisioneng.2015.04.003.

[10] S. Liu, J. Dai, A. Li, Z. Sun, S. Feng, G. Cao, Analysis of frequency characteristics and sensitivity of compliant mechanisms, Chin. J. Mech. Eng. 29 (4) (2016) 680–693, http://dx.doi.org/10.3901/CJME.2015.1215.148.

[11] S.M. Lyon, P.A. Erickson, M.S. Evans, L.L. Howell, Prediction of the first modal frequency of compliant mechanisms using the pseudo-rigid-body model, J. Mech. Des. 121 (2) (1999) 309–313, http://dx.doi.org/10.1115/1.2829459.

[12] Y.-Q. Yu, L.L. Howell, C. Lusk, Y. Yue, M.-G. He, Dynamic modeling of compliant mechanisms based on the pseudo-rigid-body model, J. Mech. Des. 127 (4) (2005) 760–765, http://dx.doi.org/10.1115/1.1900750.

[13] S. Salinic, A. Nikolić, Determination of natural frequencies of a planar serial flexure-hinge mechanism using a new pseudo-rigid-body model (PRBM) method, in: International Congress of Serbian Society of Mechanics, Vol. 6, 2017, pp. 1–11.

[14] Vedant, J.T. Allison, Pseudo-rigid body dynamic modeling of compliant members for design, in: Proceedings of the ASME International Design Engineering Technical Conferences and Computers and Information in Engineering Conference - 2019, the American Society of Mechanical Engineers, New York, N.Y., 2020, pp. 1–11, http://dx.doi.org/10.1115/DETC2019-97881.

[15] Y.-Q. Yu, Q. Li, Q.-P. Xu, Pseudo-rigid-body dynamic modeling and analysis of compliant mechanisms, Proc. Inst. Mech. Eng. C 232 (9) (2018) 1665–1678, http://dx.doi.org/10.1177/0954406217707547.

[16] Y. Zheng, Y. Yang, R.-J. Wu, C.-Y. He, C.-H. Guang, Dynamic analysis of a hybrid compliant mechanism with flexible central chain and cantilever beam, Mech. Mach. Theory 155 (2021) 104095, http://dx.doi.org/10.1016/j.mechmachtheory.2020.104095.

[17] J. Hu, T. Wen, J. He, Dynamics of compliant mechanisms using transfer matrix method, Int. J. Precis. Eng. Manuf. (2020) http://dx.doi.org/10.1007/s12541-020-00395-9.

[18] M. Ling, J. Cao, N. Pehrson, Kinetostatic and dynamic analyses of planar compliant mechanisms via a two-port dynamic stiffness model, Precis. Eng. 57 (2019) 149–161, http://dx.doi.org/10.1016/j.precisioneng.2019.04.004.

[19] N. Nesic, L. Zentner, Free vibration of compliant mechanisms consisting of Euler-Bernoulli beams, in: T. Uhl (Ed.), Advances in Mechanism and Machine Science, in: Mechanisms and Machine Science, vol. 73, Springer International Publishing, Cham, 2019, pp. 3255–3262, http://dx.doi.org/10.1007/978-3-030-20131-9_321.

[20] M. Ling, L.L. Howell, J. Cao, G. Chen, Kinetostatic and dynamic modeling of flexure-based compliant mechanisms: A survey, Appl. Mech. Rev. 72 (3) (2020) http://dx.doi.org/10.1115/1.4045679.

[21] A. Obradović, S. Šalinić, D.R. Trifković, N. Zorić, Z. Stokić, Free vibration of structures composed of rigid bodies and elastic beam segments, J. Sound Vib. 347 (347) (2015) 126–138, http://dx.doi.org/10.1016/j.jsv.2015.03.001.

[22] M. Knaebel, H. Jäger, R. Mastel, Technische Schwingungslehre: Grundlagen - Modellbildung - Anwendungen, nineth ed.., überarbeitete Auflage, in: Lehrbuch, Springer Vieweg, Wiesbaden, 2016, http://dx.doi.org/10.1007/978-3-658-13793-9.

[23] S. Linß, P. Schorr, L. Zentner, General design equations for the rotational stiffness, maximal angular deflection and rotational precision of various notch flexure hinges, Mech. Sci. (8) (2017) 29–49, http://dx.doi.org/10.5194/ms-8-29-2017.

[24] S. Linß, R. Opfermann, P. Gräser, R. Theska, L. Zentner, Nachgiebige koppelmechanismen mit optimierten festkörpergelenken für präzisionsanwendungen, 2015, http://dx.doi.org/10.17185/DUEPUBLICO/37267, DuEPublico: Duisburg-Essen Publications Online, University of Duisburg-Essen, Germany.

[25] V. Läpple, Torsion nicht kreisförmiger querschnitte, in: V. Läpple (Ed.), Lösungsbuch Zur Einführung in Die Festigkeitslehre, in: Viewegs Fachbücher der Technik, Vieweg, Wiesbaden, 2007, pp. 207–213, http://dx.doi.org/10.1007/978-3-8348-9199-0_11.

[26] M. Darnieder, F. Harfensteller, P. Schorr, M. Scharff, S. Linß, R. Theska, Characterization of thin flexure hinges for precision applications based on first eigenfrequency, in: L. Zentner, S. Strehle (Eds.), Microactuators, Microsensors and Micromechanisms, in: Mechanisms and Machine Science, vol. 96, Springer International Publishing, Cham, 2021, pp. 15–24, http://dx.doi.org/10.1007/978-3-030-61652-6_2.